Observation and Control of Transverse Energy-Transport Barrier due to the Formation of an Energetic-Electron Layer with Sheared $E \times B$ Flow

T. Cho,[1] J. Kohagura,[1] T. Numakura,[1] M. Hirata,[1] H. Higaki,[1] H. Hojo,[1] M. Ichimura,[1] K. Ishii,[1] K. Md. Islam,[1] A. Itakura,[1] I. Katanuma,[1] R. Minami,[1] Y. Nakashima,[1] T. Saito,[1] Y. Tatematsu,[1] O. Watanabe,[1] M. Yoshikawa,[1] A. Kojima,[1,*] Y. Miyake,[1] Y. Miyata,[1] K. Shimizu,[1] Y. Tomii,[1] M. Yoshida,[1,*] K. Sakamoto,[1,*] T. Imai,[1] V. P. Pastukhov,[2] S. Miyoshi,[1] and GAMMA 10 Group

[1]*Plasma Research Center, University of Tsukuba, Tsukuba, Ibaraki 305-8577, Japan*
[2]*Russian Research Center "Kurchatov Institute," Moscow, Russia*

(Received 23 December 2005; published 31 July 2006)

Off-axis electron-cyclotron heating in an axisymmetric barrier mirror produces a cylindrical layer with energetic electrons, which flow through the central cell and into the end region. The layer, producing a localized bumped ambipolar potential Φ_C, forms a strong shear of radial electric fields E_r and peaked vorticity with the direction reversal of $E_r \times B$ sheared flow near the Φ_C peak. Intermittent vortexlike turbulent structures near the layer are suppressed in the central cell by this actively produced transverse energy-transport barrier; this results in T_e and T_i rises surrounded by the layer.

DOI: 10.1103/PhysRevLett.97.055001 PACS numbers: 52.55.Jd, 52.25.Fi, 52.70.La

Anomalous cross-field plasma transport is one of the most critical issues in magnetic plasma confinement for fusion as well as in physics of magnetized plasmas in general. Previously, some regimes with reduced anomalous transverse transport have been observed in tokamaks (see Ref. [1], and references therein). It is of essential importance for the progress in fusion programs to control the transition toward such regimes.

According to recent theories [1], transition to an H mode with improved plasma confinement or the formation of internal transport barriers (ITB) in toroidal systems is associated with an increase in nonuniform radial electric fields E_r and a corresponding enhancement of sheared plasma rotation. Remarkably, the low-frequency (LF) plasma turbulence and the resultant anomalous transport observed in various devices for magnetic plasma confinement exhibit rather common features. Recently, intermittent LF turbulent vortex structures and effects of their suppression by strongly sheared plasma rotation were observed in the GAMMA 10 tandem mirror [2–4]. The suppression of turbulence and the associated significant reduction in cross-field transport observed in GAMMA 10 show behaviors that are similar to those seen for L-H transitions in tokamaks. Fortunately, mirror devices, having open-ended regions, provide intrinsic important advantages in terms of the control of radial-potential or sheared $\boldsymbol{E} \times \boldsymbol{B}$ rotation profiles on the basis of axial particle-loss control [2–9].

In this Letter, we present the results obtained by means of *actively controllable* modification of radial potential or E_r shear profiles in GAMMA 10. An alternative application of electron-cyclotron heating (ECH) with an *off-axis resonance location* facilitates the formation for a profile of plasma rotation with a radially localized high-vorticity layer. Formation of radial transport barrier, which has similar properties to ITB in toroidal plasmas [1], has been observed in the vicinity of the high-vorticity layer in GAMMA 10. Decoupling and reduction of intermittent turbulent structures across the transport-barrier region are visually demonstrated with temperature rises in the core plasmas.

GAMMA 10, which is a minimum-B anchored tandem mirror with outboard axisymmetric plug and barrier cells [2–4,7,10–15], has an axial length (L_z) of 27 m and the vacuum vessel of 150 m^3. In the central cell ($L_z = 6$ m, limiter diameter of 36 cm, and magnetic fields $B_z = B_m$ at the midplane of 0.405 T with a mirror ratio R_m of 5.2.), ion cyclotron heating (30 kW at 6.36 MHz for central-cell hot-ion production, and 30 kW at 9.9 or 10.3 MHz for anchor stabilization) is applied. The plug and barrier cells are axisymmetric mirrors with $L_z = 2.5$ m, $B_m = 0.497$ T, and $R_m = 6.2$ for standard operations. However, in the present experiments, 4.75% higher B_m (0.519 T) is applied in the barrier cell for off-axis resonant ECH to produce the cylindrical energetic-electron layer. Gyrotron power of 120 kW at 28 GHz is injected into a single (east) barrier cell alone. No additional ECH is applied, thereby simplifying the experimental situations.

Various fluctuation diagnostics including a movable microwave interferometer, the Fraunhofer-diffraction method [15], two sets of our developed 50-channel soft x-ray tomography detectors using microchannel plates [2–4,10–12,16] in the central-cell midplane, eight Langmuir probes [2] for wave phasing and coherence diagnostics, heavy-ion (Au^0) beam probes (HIBP) [17] and eight sets of ion-energy-spectrometer (IES) arrays [13], and simultaneous potential diagnostics with HIBP and IES show consistently the same characteristics as described below. Energetic-electron currents are observed with a radially movable conventional end-loss analyzer (ELA) and ELA arrays [11,14] at the west end.

Under these operational conditions, the off-axis resonant barrier-cell ECH produces a cylindrical layer with high-

energy electrons of ≈2 keV and a population of the order of 10^{-5} with respect to the total density in the layer. Thus, beta-value effects and slowing down plasma heating are negligible. The cylindrical layer is centered at $r_c = 5.5$ cm with half-width of approximately 1.5 cm. The layer is axially formed throughout the device; i.e., energetic electrons present in the layer due to the (east) barrier-cell ECH flow through the central cell and escape into the open-ended region.

A potential difference between the central cell and floated end plates in the energetic-electron layer forms so as to prevent longitudinal losses of high-energy electrons. As a result, nonmonotonic bumped-shape radial profile of plasma potential Φ_C forms in central cell. The solid and dashed curves in Fig. 1(a) show the Φ_C profiles in the presence and absence of the energetic-electron layer, respectively. The radial position of the cylindrical layer ($4 < r_c < 7$ cm) and the electron-current density profile observed with the radially movable ELA [11,14] are shown as shaded regions. The Φ_C data from the central-cell HIBP [17] and (west) IES arrays [13] in the presence and absence of the layer are plotted with solid and open circles, respectively. The profiles of the rotational frequency $\Omega(r_c) = -E_r/(r_c B)$, which characterizes the azimuthal plasma drift flow, are shown in Fig. 1(b). The solid curve shows Ω profile in the presence of the energetic-electron layer. The curve changes sign at the Φ_C peak location, $r_c \approx 7$ cm $\equiv r_p$, which represents the *direction reversal* of the $\boldsymbol{E} \times \boldsymbol{B}$ azimuthal (θ) drift flow across $r_c = r_p$ with the consequence that the oppositely directed $\boldsymbol{E} \times \boldsymbol{B}$ sheared drift flows separate plasmas into two regions at $r_c = r_p$.

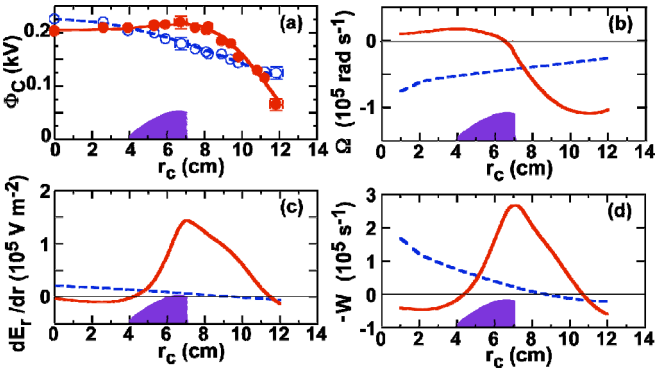

FIG. 1 (color online). (a) Central-cell potential data from HIBP and IES arrays are plotted with solid and open circles, respectively, along with solid and dashed fitting curves for the presence and absence of the energetic-electron layer, respectively. The inserted shaded region shows the observed profile of the electron-current density [$4 < r_c < 7$ cm]. (b) The angular velocity, which shows the direction reversal of the $\boldsymbol{E} \times \boldsymbol{B}$ azimuthal drift flow across the bumped locations at $r_c = r_p \approx 7$ cm of (c) E_r shear and (d) dynamic vorticity, is plotted in the presence of the energetic-electron layer (solid curves).

Further essential features are found in the behaviors of the radial plots of the E_r shear [Fig. 1(c)] and the dynamic vorticity W [Fig. 1(d)]. As shown in Ref. [18], W plays a role of the canonical momentum of such rotational motion in magnetized plasmas with nonuniform density. It provides a natural generalization of the vorticity vector $\boldsymbol{w} = \boldsymbol{\nabla} \times \boldsymbol{V}$, which is well known as a canonical momentum and as a measure of velocity shear in dynamics of incompressible fluids. The z component of normalized dynamic vorticity $W = [\boldsymbol{\nabla} \times (n\boldsymbol{V}_E)]_z/n_0 = d/dr_c[n r_c^2 \Omega]/(n_0 r_c)$ (where n_0 is the on-axis density) is chosen to characterize $\boldsymbol{E} \times \boldsymbol{B}$ velocity ($\boldsymbol{V}_E$) shear in our experiments [2–4]. In the presence of the energetic-electron layer, the Φ_C profile in Fig. 1(a), which leads to a rapid change in Ω [Fig. 1(b)], corresponds to significant bumps in the dE_r/dr_c and W profiles in Figs. 1(c) and 1(d), respectively.

To investigate the effects of the formation of this energetic-electron layer on the behavior and structure of turbulent plasmas [Fig. 2(a)], contours of the central-cell soft x-ray brightness I_{sx} are shown [see Figs. 2(a) and 2(c) before and during ECH, respectively]. The "hot-colored"

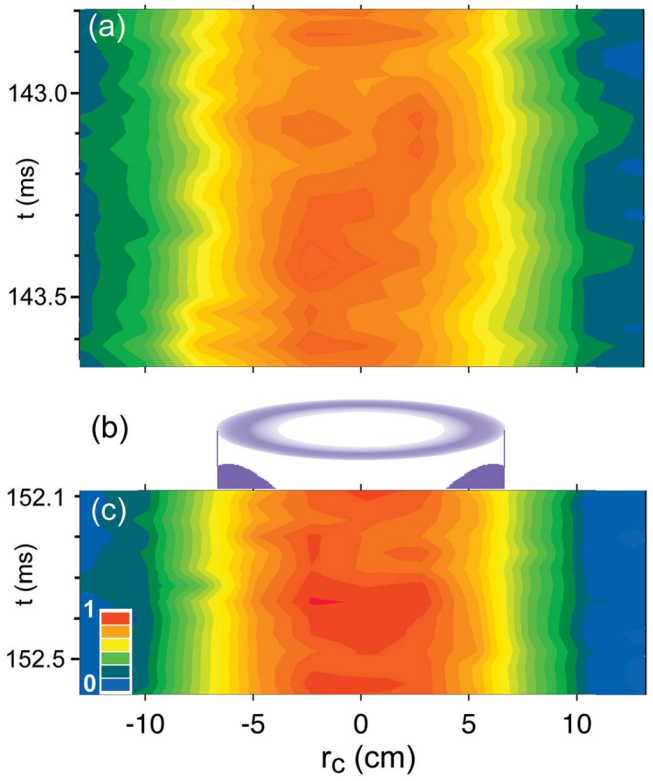

FIG. 2 (color). Contours of central-cell x-ray brightness in (a) the absence and (c) presence of (b) cylindrically shaped energetic-electron-layer formation due to off-axis barrier-cell ECH. The hot-colored areas show higher plasma-pressure locations. Strong turbulence with vortexlike structures continues to exist at $r_c < 4$ cm in (a) and (c). However, a quietly suppressed region in (c) is observed in the energetic-electron layer [$5 < r_c < 7$ cm; see (b)] and the outer surrounding cylindrical layer ($7 \leq r_c < 10$ cm); ($I \propto n_e n_i T_e^{2.3}$).

regions indicate higher plasma-pressure locations (for more detail, see Refs. [2–4]). The radial position of the cylindrical layer during the formation period with the barrier-cell ECH ($t > 149.2$ ms) is illustrated in Fig. 2(b). One can find spatially and temporally varied intermittent turbulent vortexlike structures before the layer formation [Fig. 2(a)]. The turbulent structures are still rather high in the plasma core region, whereas they are significantly reduced in the layer and the outer region. In fact, in these regions, small temporal variations of the contours are observed during ECH; that is, almost *parallelly directed* contours to the t axis show quite small radial fluctuations of turbulence with time. [Compare the yellow or light-orange-colored region in Fig. 2(a) with those in Fig. 2(c), together with the surrounding outer green-colored region ($7 \leq r_c < 10$ cm).]

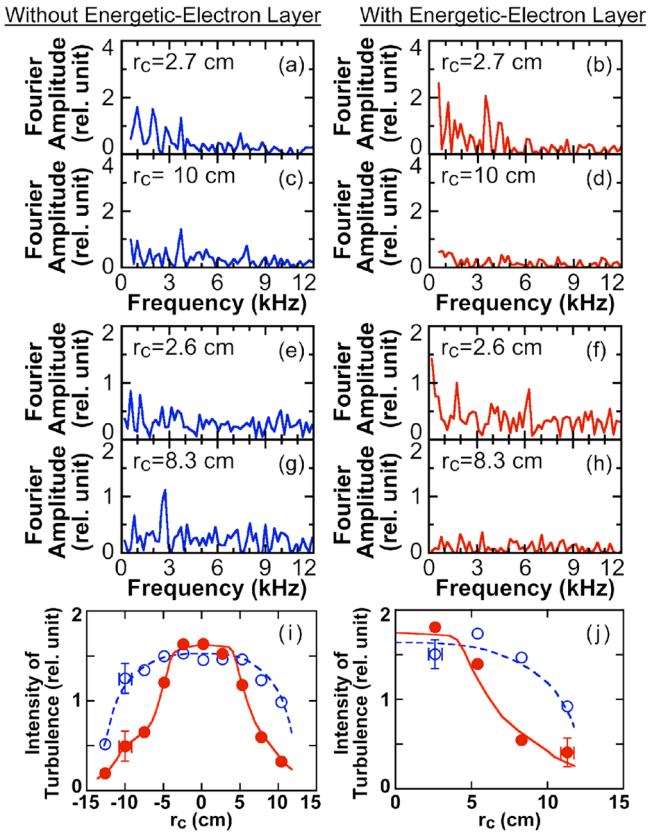

FIG. 3 (color online). Fourier amplitudes of (a)–(d) the central-cell x-ray signals from Fig. 2 and (e)–(h) those of ions from the IES arrays are plotted at various r_c values. The data sets are obtained in the absence [(a),(c),(e),(g)] and presence [(b),(d),(f),(h)] of the cylindrical energetic-electron layer [Fig. 2(b)]. Frequency-integrated amplitudes over the broadband turbulent fluctuations from the x-ray and IES array detectors are summarized in (i) and (j), respectively. Solid and open circles correspond to the cases with and without the layer formation, respectively. A significant reduction in turbulence is attained in the energetic-electron layer and outside the layer ($5 < r_c < 10$ cm). These behaviors are consistently found in Fig. 2.

In Fig. 3, Fourier analyses of both central-cell x-ray signals in Fig. 2 and in the ion signals with IES arrays [13] are presented. The Fourier amplitudes of the x rays at $r_c = 2.7$ and 10 cm without and with the energetic-electron-layer formation (around $t = 146.5$ and 152.5 ms) are shown in Figs. 3(a)–3(d), respectively. Similarly, those from the IES array at $r_c = 2.6$ [Figs. 3(e) and 3(f)] and 8.3 cm [Figs. 3(g) and 3(h)] in the absence [Figs. 3(e) and 3(g)] and presence [Figs. 3(f) and 3(h)] of layer formation are presented. The turbulent spectra (see Refs. [2–4]) at any r_c without the layer [Figs. 3(a), 3(c), 3(e), and 3(g)], as well as in the core region with the layer [Figs. 3(b) and 3(f)] are similarly observed for both x-ray and ion signals. On the other hand, the turbulence levels are significantly reduced with the layer formation [Figs. 3(d) and 3(h)].

The frequency-integrated amplitudes over the broadband turbulent fluctuations from the x-ray and IES array detectors at various radii [2–4] are summarized in Figs. 3(i) and 3(j), respectively. The solid and open circles in Figs. 3(i) and 3(j) correspond to the cases with and without the energetic-electron-layer formation, respectively. As one can see in both figures, a significant reduction of the turbulence fluctuations is attained in and outside the energetic-electron layer ($5 < r_c < 10$ cm). These behaviors are consistently observed for the signals in Fig. 2; that is, a high level of turbulence persists at $r_c < 4$ cm (i.e., the core region inside the layer) either with or without the layer [Figs. 2(a) and 2(c), respectively], although quietly suppressed regions are generalized in the higher population region of the energetic electrons ($5 < r_c < 7$ cm), as well as in the externally surrounding cylindrical region ($7 \leq r_c < 10$ cm) [Fig. 2(c)].

From these data, it appears that, even in the presence of the layer, there exists a high level of turbulent fluctuations in the core region with a weakly sheared small W ($r_c <$ 4 cm), while a quiet regime with a low level of fluctuation

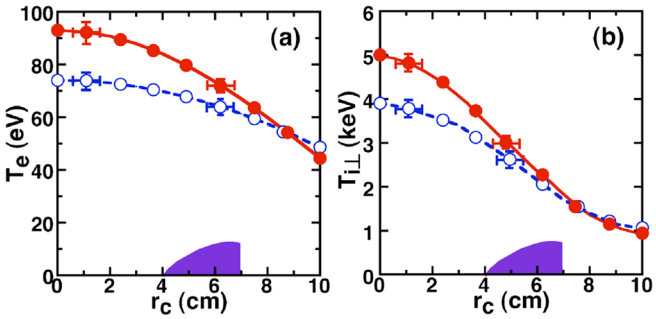

FIG. 4 (color online). The solid and dashed curves show (a) T_e and (b) T_i profiles from x-ray and charge-exchanged particle analyses in the presence and absence of the energetic-electron layer (illustrated as shaded regions), respectively. Steep gradients are noted for both T_e and T_i in a large W regime along with rather flat and higher T_e and T_i in the inner region surrounded by the layer. For simplicity, neither plug nor central ECH for direct bulk-electron heatings is injected.

is observed in and outside the layer ($5 < r_c < 10$ cm), where W increases to a peak at $r_c = 7$ cm.

As one can find in Fig. 2, the steps of the contours in $r_c < -5$ cm and $r_c > 5$ cm in Fig. 2(a) are wider and more gradual than those in Fig. 2(c) having more strongly sheared E_r or larger W. [In particular, compare the yellow-colored step width near $r_c = 7$ cm in Fig. 2(c), which has maximum W, to the yellow-step width in Fig. 2(a).] More directly, comparisons of the T_e and T_i profiles are shown in Figs. 4(a) and 4(b), respectively, from the x-ray [10–12,19–22] and charge-exchange particle analyses [23]. As expected from the aforementioned comparison in Fig. 2, one can confirm steep gradients for both T_e and T_i in this large W regime along with the resulting higher T_e and T_i in the core region surrounded by this steep gradient layer having a strong shear [see Figs. 1(c) and 1(d)]. These findings of radially improved T_e and T_i profiles, surrounded by the localized sheared flow layer, allow us to collaborate analogical similarity studies of radial transport-barrier formation in toroidal devices [1]. For instance, local heating on a magnetic surface (with some radial local losses) is a candidate for actively producing similar ambipolar potential bump and barrier.

These results allow us to interpret that large-scaled turbulence typically exists in a standard regime that has a radially smooth profile of a weakly sheared plasma rotation. Stochastic vortexlike structures [Fig. 2], with characteristic scales comparable with the plasma radius, dominate the turbulence and causes enhanced radial heat transport. Experimental results show that the presence of a high W layer leads to the suppression of turbulent fluctuations, and forms steep T_e and T_i gradients across the layer [Fig. 4]. Furthermore, the large-scaled vortices localized in the plasma core and turbulence at the plasma edge (e.g., the probe diagnostics) appear to be independent of each other. This decoupling of dominant structures is an alternative example of reduction of the radial correlation length due to sheared flows [1].

In Fig. 4, T_e rises in the core region by reduction of the effective radial thermal diffusivity $\chi_{e\perp}$ in the high W layer to the classical value ≈ 0.003 m^2 s^{-1} together with axial plugging by floated end-plate potential depth ($\approx 3T_e$) [5,7]. In addition, enhancement of T_i for central-mirror ions is well interpreted by the absence of appreciable anomalous ion radial losses across the layer and by the classical electron drag. Continuity of total transverse fluxes necessarily leads to the local enhancement of temperature gradients [Fig. 4]. In fact, the T_e gradient becomes steeper by a factor of 2 in the high W region ($5 < r_c < 10$ cm), while the temperature profiles in the weakly sheared plasma core remain rather flat. Following the conventional definition of ITB [1], we interpret these effects as alternative formation of an internal transport barrier in the area that has an actively controlled high-velocity shear.

*Permanent Address: Japan Atomic Energy Agency, Naka, Ibaraki, Japan.

[1] Y. Kishimoto *et al.*, Nucl. Fusion **40**, 667 (2000); S. Ide and the JT-60 Team, *ibid.* **45**, S48 (2005); J. W. Connor *et al.*, Plasma Phys. Controlled Fusion **42**, R1 (2000); P. H. Diamond *et al.*, Plasma Phys. Controlled Fusion **47**, R35 (2005); J. C. Perez *et al.*, Phys. Plasmas **13**, 055701 (2006).
[2] T. Cho *et al.*, Phys. Rev. Lett. **94**, 085002 (2005).
[3] T. Cho *et al.*, in *Proceedings of 20th IAEA Fusion Energy Conference, Vilamoura, 2004* (IAEA, Vienna, 2004).
[4] T. Cho *et al.*, Nucl. Fusion **45**, 1650 (2005).
[5] See R. F. Post, Nucl. Fusion **27**, 1579 (1987) for a review of mirrors; Trans. Fusion Sci. Tech. **43**, No. 1T, 195 (2003).
[6] D. D. Ryutov, *Reviews of Plasma Physics* (Consultants Bureau, New York 1987), Vol. 13, pp. 93–202.
[7] S. Miyoshi *et al.*, Fiz. Plazmy **23**, 781 (1997) [Plasma Phys. Rep. **23**, 723 (1997)].
[8] V. P. Pastukhov, Nucl. Fusion **14**, 3 (1974); R. H. Cohen *et al.*, Nucl. Fusion **18**, 1229 (1978); **19**, 1295 (1979).
[9] A. C. England *et al.*, Trans. Fusion Sci. Tech. **43**, No. 1T, 73 (2003); M. Kwon *et al.*, *ibid.* **43**, No. 1T, 23 (2003).
[10] T. Cho *et al.*, Phys. Rev. Lett. **64**, 1373 (1990).
[11] T. Cho *et al.*, Phys. Rev. A **45**, 2532 (1992).
[12] T. Cho *et al.*, Nucl. Fusion **27**, 1421 (1987).
[13] M. Yoshida *et al.*, Rev. Sci. Instrum. **74**, 1909 (2003).
[14] T. Cho *et al.*, Nucl. Fusion **28**, 2187 (1988).
[15] A. Mase *et al.*, Phys. Rev. Lett. **64**, 2281 (1990); Nucl. Fusion **31**, 1725 (1991).
[16] M. Hirata *et al.*, Nucl. Instrum. Methods Phys. Res., Sect. B **66**, 479 (1992).
[17] K. Ishii *et al.*, Rev. Sci. Instrum. **60**, 3270 (1989).
[18] V. P. Pastukhov, Plasma Phys. Rep. **31**, 577 (2005); JETP Lett. **82**, 356 (2005).
[19] J. Kohagura *et al.*, Phys. Rev. E **56**, 5884 (1997); T. Cho *et al.*, Nucl. Instrum. Methods Phys. Res., Sect. A **348**, 475 (1994).
[20] T. Cho *et al.*, Phys. Rev. Lett. **86**, 4310 (2001).
[21] T. Cho *et al.*, Nucl. Fusion **41**, 1161 (2001).
[22] T. Cho *et al.*, Nucl. Fusion **43**, 293 (2003).
[23] T. Numakura *et al.*, Plasma Phys. Controlled Fusion **45**, 807 (2003); Appl. Phys. Lett. **76**, 146 (2000).